GEOPHYSICAL TRANSACTIONS 1988
Vol. 33. No. 3–4. pp. 267–293

COMPUTER SIMULATION OF ^{252}Cf NEUTRON FIELDS IN BAUXITE WELL LOGGING

Iván BALOGH*

The distribution of neutron fields is examined by the computer modelling of neutron transport in bauxitic rocks of high hydrogen content. The modelling program, based on the Monte Carlo method is introduced and tested by known measurement data. Results of computations for typical bauxitic rocks are presented according to which epithermal and thermal neutrons have exponential distributions. With a knowledge of the epithermal and thermal neutron distributions the $\xi\Sigma_i$, Σ_s and Σ_a neutron physical parameters may be calculated. These parameters are in direct linear relation with the chemical composition of a given medium. The distorting effects on the neutron field of the probe and the borehole (wet or dry) is demonstrated qualitatively.

Keywords: bauxite prospecting, well logging, neutron logging, simulation, computer programs, macroscopic cross section

1. Introduction

Bauxites in Hungary are deposited on a karstic basement. During drilling, the drilling mud is often completely lost whereupon the hole is saved from collapse by casing. Thus, drilling for bauxite means more difficult conditions for well logging than for other materials because three-quarters of the measurements fall on cased or dry intervals. Due to these circumstances well logging in bauxite prospecting in Hungary has been based on nuclear logging since the beginning. Recently, nuclear well-logging methods have started to develop rapidly. In our case even the in situ determination of the chemical composition of bauxites in the borehole may be set as a long-term objective. The solution of the so-called direct problem must be the first step towards our objective, in other words the study of the behaviour of nuclear radiation fields in bauxite. Here, we deal with neutron fields induced in bauxitic rocks.

2. Possibilities of analytical and numerical computation of neutron fields in bauxite well logging

The so-called transport-equation, an integro-differential equation of seven variables, describes the distribution of neutrons according to space, energy and angle [SZATMÁRY 1971]. This equation may analytically be solved only in special cases: the most important of these are the solution according to Fermi's age

* Hungalu Prospecting Company, POB 31, Balatonalmádi, H–8221, Hungary
Manuscript received: 13 July, 1987

theory and the diffusion one. Low hydrogen content is among the initial conditions of both solutions; however, Hungarian bauxites have a high hydrogen content. The main minerals that constitute bauxites contain much hydrogen themselves (see *Table I* after BÁRDOSSY 1977, BETECHTIN 1964). Furthermore, these bauxites are strongly hygroscopic, their percentage of water is between 16 and 20% of the weight in the in-mine state [BARNABÁS 1966]. Thus, the hydrogen porosity of a high quality gibbsitic bauxite may reach 80% and that of the good boehmitic bauxites is around 60% *(Table II)*. This means that neither the diffusion approach nor Fermi's age theory can give a satisfactory solution. More accurate results may be obtained by the so-called multigroup diffusion method [SZATMÁRY 1971]. If one divides the energy scale into intervals the diffusion approach may be assumed valid even for a medium rich in hydrogen if the intervals are short enough. In this case a system of diffusion differential equations is to be solved where the number of equations corresponds to the number of intervals, i.e. to the number of groups. The source side of the equations of the lower groups will depend on all the groups having higher energy due to the presence of hydrogen [FEHÉR 1984]. The system of equations has an analytical solution in one dimension but with more complicated geometry only numerical methods work. At this stage, however, the necessary amount of computing time and memory capacity is comparable to those needed for the exact computer modelling of neutron transport. In view of this and because the modelling programs are simple and highly flexible, and because the borehole and the construction of the probe can easily be taken into account a Monte Carlo simulation program utilizing a Commodore 64 was written for the task.

Mineral	Chemical formula	Density (g/cm^3)	Hydrogen porosity (%)
Boehmite	AlOOH	3.035	45.6
Gibbsite	$Al(OH)_3$	2.35	81.4
Kaolinite	$Al_4(OH)_8Si_4O_{10}$	2.59	36.2
Calcite	$CaCO_3$	2.71	–
Siderite	$FeCO_3$	3.8	–
Pyrite	FeS_2	5.05	–
Goethite	FeOOH	4.2	42.6
Haematite	Fe_2O_3	5.1	–
Rutile	TiO_2	4.25	–
Anatase	TiO_2	3.9	–
Water	H_2O	1	100

Table I. The rock-forming minerals of Hungarian bauxites, their density and hydrogen prorosity

I. táblázat. A hazai bauxitok fő kőzetalkotó ásványai, sűrűségük és hidrogén porozitásuk

Таблица I. Главные породообразующие минералы, плотность и водородная пористость отечественных бокситов.

Mineral \ Rock code		0	1	2	3	4	5	6	7
Boehmite	[vol. %]	0	0	0	40	15	15	0	20
Gibbsite	[vol. %]	0	50	20	0	0	15	0	0
Kaolinite	[vol. %]	0	2	30	5	35	15	40	2.5
Calcite	[vol. %]	0	0.5	1	1	1	0.5	0	50
Pyrite	[vol. %]	0	0	0	0	0	13	0	0
Goethite	[vol. %]	0	2	3	4	3	5	15	2
Haematite	[vol. %]	0	4	7	8	7	0	5	4
Rutile/Anatase	[vol. %]	0	0.5	1	1	1	1	0	0.5
Water	[vol. %]	100	41	38	41	38	35.5	40	21
Density	[g/cm^3]	1	1.96	2.18	2.4	2.29	2.47	2.32	2.55
Hydrogen porosity	[%]	100	83.3	66.42	62.8	58.8	62.1	60.9	31.9

Table II. Mineral composition of rocks involved in the simulation of neutron fields
Code numbers: 0 — water; 1 — gibbsitic bauxite; 2 — clayey, gibbsitic bauxite; 3 — boehmitic bauxite; 4 — clayey, boehmitic bauxite; 5 — pyritic bauxite; 6 — clay; 7 — bauxite mixed with detrital limestone

II. táblázat. A neutronterek szimulációja során modellezett kőzetek ásványi összetétele
Kódszámok: 0 — víz; 1 — gibbszites bauxit; 2 — agyagos gibbszites bauxit; 3 — böhmites bauxit; 4 — agyagos böhmites bauxit; 5 — pirites bauxit; 6 — agyag; 7 — mészkőtörmelékes bauxit

Таблица II. Минеральный состав пород, моделированных при симуляции нейтронных полей.
Кодовые номера: 0 — вода, 1 — гиббситовый боксит, 2 — глинистый гиббситовый боксит, 3 — бёмитовый боксит, 4 — глинистый бёмитовый боксит, 5 — пиритизированный боксит, 6 — глина, 7 — боксит с обломками известняков.

3. Main features of the simulation program

The essence of the modelling of neutron fields is the computer simulation of the transport of single neutrons based on the simple laws of neutron physics and on probability considerations, and the statistical testing of the behaviour of an adequate number of simulated neutrons. Many publications are available on Monte Carlo methods and their applications in nuclear well logging [YERMAKOV 1975, SZOBOL 1981, DENISHIK et al. 1962, PSHENICHNYY 1982, FEHÉR 1984, KHISAMUTDINOV et al. 1985] so only the main features of the program are enumerated here.

The initial energy of the neutrons is determined by the energy spectrum of the modelled source. The energy spectrum of two sources having the same neutron yield is shown in *Fig. 1.* One is a Ra–Be source of 1 GBq activity (dotted line), the other is a ^{252}Cf source of 3 MBq activity (continuous line). The ^{252}Cf source has a smoother spectrum than that of the Ra–Be source. Bearing in mind the relatively low energies and the medium atomic weights only scattering was

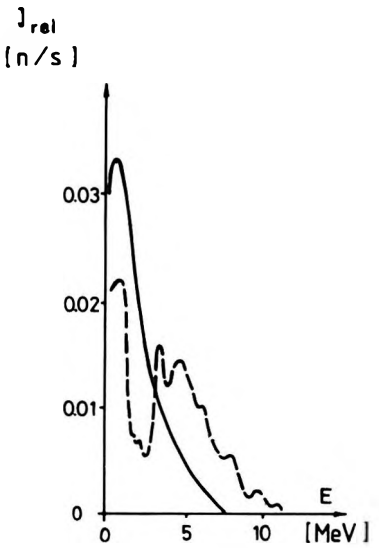

Fig. 1. Energy spectra of ^{252}Cf (continuous line) and Ra–Be (dotted line) neutron sources [after Radiation Sources 1974, SZABÓ—SIMONITS 1973, and KARDON et al. 1971]

1. ábra. Neutronforrások energia spektrumai: ^{252}Cf — folytonos vonal, Ra–Be — szaggatott vonal

Рис. 1. Энергетический спектр источников нейтронов ^{252}Cf—прерывситая линия; Ra–Be—сплошная линия.

taken into account from the possible interactions in the fast range. Angular distribution of scattering was assumed to be isotropic in the mass-centrical coordinate system. Values of the microscopic fast cross-sections were taken from the literature [NIKOLAYEV and BAZAZYANTS 1972, ALLEN 1960]. In the actual calculations the average values of the fast cross-sections weighted by 1/E (E: energy) were used except for hydrogen. The boundary of the fast range was defined as being at the beginning of the thermal Maxwell spectrum, i.e. at 0.1 eV *(Fig. 2)*.

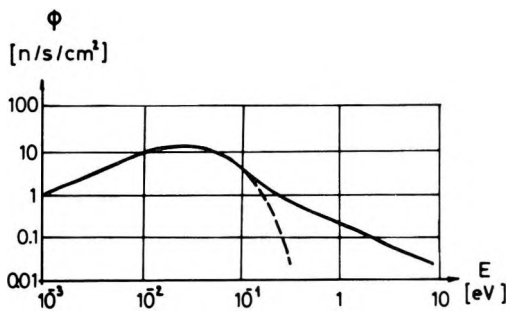

Fig. 2. Function of the fast and the thermal range of neutron flux. The part of the Maxwell spectrum which joins the fast range is indicated by dotted line [from SZATMÁRY 1971]

2. ábra. Neutronfluxus gyors és termikus tartományának csatlakozása. A termikus Maxwell-spektrum gyors tartományhoz csatlakozó szakaszát szaggatott vonal jelzi

Рис. 2. Стыковка быстрого и термического диапазонов нейтронного потока. Интервал стыковки термического спектра Максвелла к быстрому диапазону обозначен прерывистой линией.

In the modelling project resonance neutrons captured by indium and cadmium foils, and epithermal neutrons measured by a shielded He^3 proportional counter had to be modelled as well. Resonance neutrons were recorded by the program when crossing the 1.44 and 0.1 eV energy levels, thus, in fact the slowing down densities belonging to the corresponding energies were obtained. The flux of epithermal neutrons that could be measured by the proportional counter were recorded in the 1.0–0.1 eV energy interval during simulation.

In the thermal range scattering and absorbing interactions were taken into account. Scattering was regarded as being isotropic in the so-called laboratory system of coordinates, too, because the velocities of thermal neutrons and colliding nuclei are commensurable. The corresponding values of the microscopic cross-sections were taken from the literature [NAGY 1971]. There are considerable differences in the literature data regarding the thermal cross-section for scattering of hydrogen (38 barn in NAGY 1971, 20.3 barn in PSHENICHNYY 1982). On the other hand, the literature values of the thermal diffusion-length are very similar, viz. $L_d \approx 2.7$ cm. Calculating with that value and checking it by modelling the result gave 28 barn for the effective thermal cross-section for the scattering of hydrogen.

To trace the trajectories of neutrons the method given by DENISHIK et al. [1962] was used. The change in direction caused by scattering may be described by two rotation which have axes perpendicular to each other. Let us denote the product matrix of the multiplication of the two rotations by T_i at the i-th collision. Then vector $\vec{r}_i$ determining the direction of the next free path of the neutron may be obtained from the initial direction-vector $\vec{r}_0$ as follows:

$$\vec{r}_i = T_0 T_1 \ldots T_{i-1} T_i \vec{r}_0$$

that is

$$\vec{r}_i = P_{i-1} T_i \vec{r}_0$$

where

$$P_{i-1} = \prod_{k=0}^{i-1} T_k$$

Once the direction changes and the covered free paths are known, the position of the neutrons can be determined. Inhomogeneous material of complicated geometry may cause difficulties while modelling the free path because the total macroscopic cross-section (Σ_t), which determines the free path, becomes a function of place. In this case it is expedient to define a fictive cross-section of maximum value Σ_t^0 for the whole space under investigation [SZGŁOŁ 1981]. Thus, the free path is computed by the same algorithm in the whole space. In the j-th part of the space, however, the collision will be fictive with a probability of

$$K^j = \frac{\Sigma_t^0 - \Sigma_t^j}{\Sigma_t^0}$$

i.e. the energy and direction of movement of the neutron remain unchanged. The position and behaviour of the neutrons are easily traceable by this method in any medium having complicated geometry and chemical composition.

The Monte Carlo program was written in the above described way, see *Figs. 3* and *4*. Firstly the boundary and initial conditions — i.e. the geometrical structure, the chemical composition of the medium and the energy spectrum of the radiation source — are defined. The neutron is "born" in a radioactive source placed at the origin and it has an initial energy which is generated according to the spectrum of the source. The initial value of its direction-vector and P_{i-1} transformation matrix is unity. The initial direction of its trace gets a random value because the value of the first T transformation matrix is generated randomly. The fictive free path is independent of energy and space domain. The real free path is depending on energy and space domain and on whether the collision was real or fictive. In the case of a real collision the energy and direction of the neutron will change depending on the target nucleus. If the energy of the neutron decreases below 0.1 eV it will move over to the thermal range. In the thermal range the fictive free path is also independent of the space domain and the real free path will again be determined by the fictive and real collisions. The energy of the neutron is not changed by scattering and the distribution of scattering direction is independent of the target nucleus and isotropic. Absorption ends the "life" of neutrons. If insufficient neutrons are modelled the program steps to point A to generate a new neutron.

4. Testing of the simulation program by published data

Many publications discuss the space distribution of neutrons and experimental data are also found in a number of them. Most experiments deal with water but data concerning, for example, sandstone, are also available. Thus we could test our program by published data.

At first the field of a Na–γ–Be source placed in water — a homogeneous, isotropic medium — was simulated. The measured data corresponding to that model were published by DENISHIK et al. [1962]. The measurements were performed with the help of indium foil, thus, epithermal neutrons of 1.44 eV energy were involved. The initial energy was taken to be 0.966 MeV and the first, fast part of the program was run with 1.44 eV threshold-energy. The results of the computation involving 3900 neutrons can be seen in *Fig. 5*. The distance from the source is on the horizontal axis, the number of neutrons on concentrical, spherical surfaces at a distance r from the source is shown on the vertical axis. The scale is logarithmic. Measured data are marked by continuous line and dots represent the computed averages for 2 cm thick spherical shells.

Fig. 3. Block diagram of the Monte Carlo simulation program in the fast range

3. ábra. A szimulációs (Monte Carlo) program blokkvázlata a gyors tartományban

Рис. 3. Блок-схема симуляционной программы Монте Карло в быстром диапазоне.

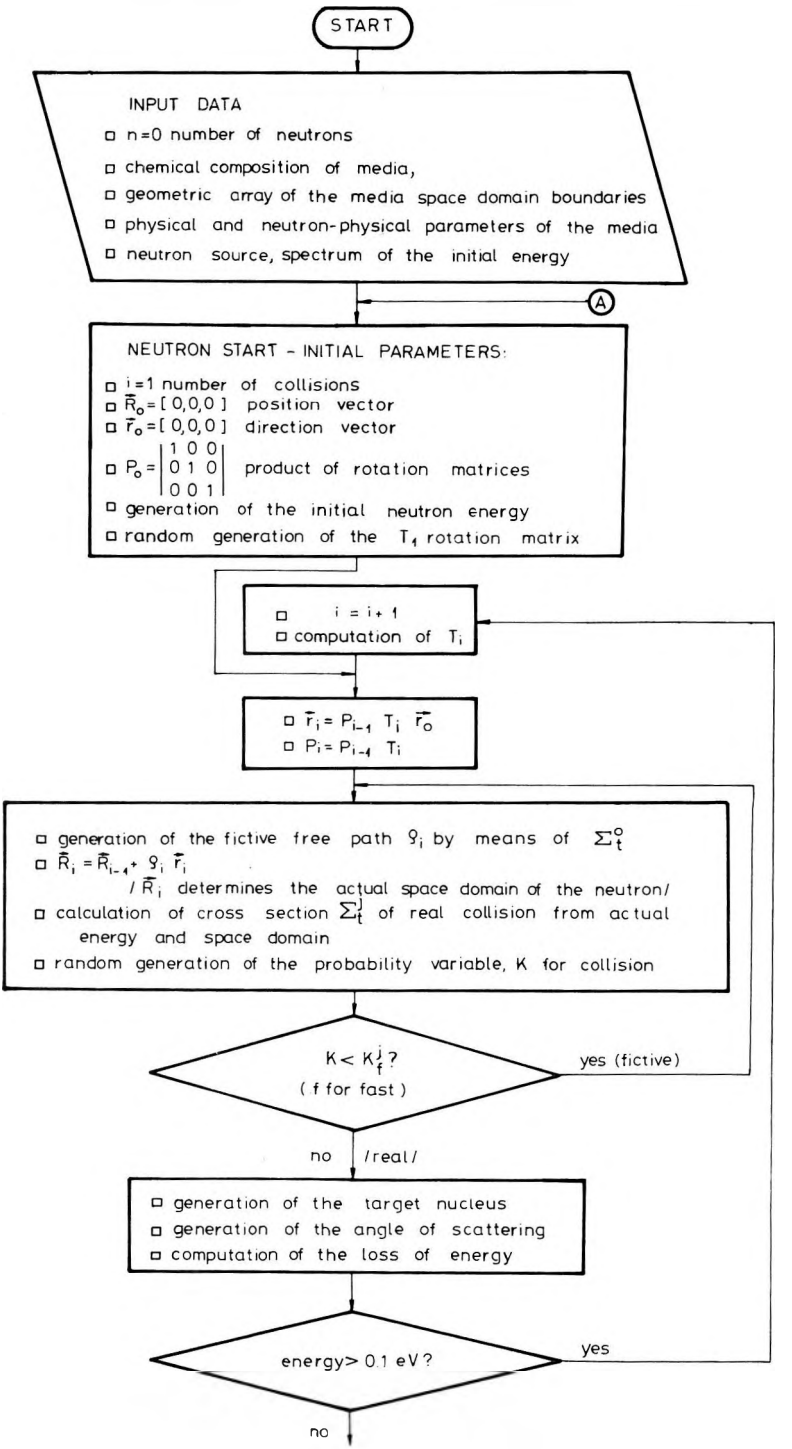
START
INPUT DATA
□ n=0 number of neutrons
□ chemical composition of media,
□ geometric array of the media space domain boundaries
□ physical and neutron-physical parameters of the media
□ neutron source, spectrum of the initial energy
A
NEUTRON START - INITIAL PARAMETERS:
□ i=1 number of collisions
□ $\vec{R}_o$=[0,0,0] position vector
□ $\vec{r}_o$=[0,0,0] direction vector
□ P_o = | 1 0 0 | / | 0 1 0 | / | 0 0 1 | product of rotation matrices
□ generation of the initial neutron energy
□ random generation of the T_1 rotation matrix
□ i = i+1
□ computation of T_i
□ $\vec{r}_i = P_{i-1}\ T_i\ \vec{r}_o$
□ $P_i = P_{i-1}\ T_i$
□ generation of the fictive free path ϑ_i by means of Σ_t^o
□ $\vec{R}_i = \vec{R}_{i-1} + \vartheta_i\ \vec{r}_i$
/$\vec{R}_i$ determines the actual space domain of the neutron/
□ calculation of cross section Σ_t^j of real collision from actual energy and space domain
□ random generation of the probability variable, K for collision
K < K_f^j ?
(f for fast)
yes (fictive)
no /real/
□ generation of the target nucleus
□ generation of the angle of scattering
□ computation of the loss of energy
energy > 0.1 eV ?
yes
no

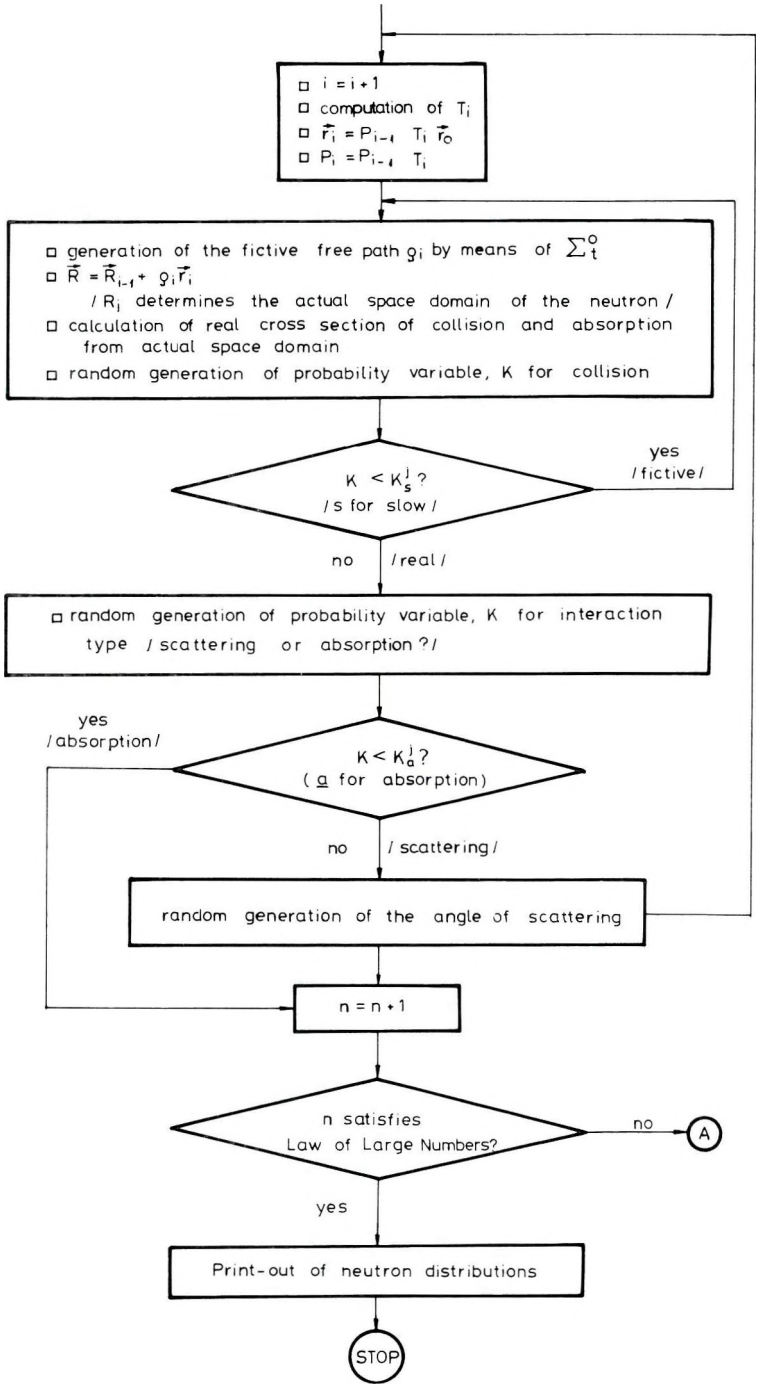

Fig. 4. Continuation of Fig. 3: Block diagram of the Monte Carlo simulation program in the thermal range

4. ábra. A 3. ábra folytatása: a szimulációs program a termikus tartományban

Рис. 4. Продолжение рис. 3. — симуляционная программа в термическом диапазоне.

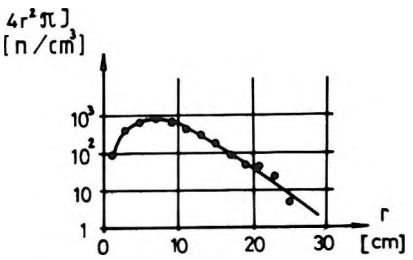

Fig. 5. Epithermal neutron distribution of Na–γ–Be neutron source measured in water by indium foil (continuous line) and computed by the simulation program (dots)

5. ábra. Na–γ–Be neutronforrás körüli epitermikus neutroneloszlás vízben, indium fóliával mérve (folytonos vonal), és a szimulációs programmal számítva (pontok)

Рис. 5. Распределение эпитермических нейтронов от источника Na–γ–Be в воде при измерении индиевой фольгой (сплошная линия) и при расчете симуляционной программой (пунктир).

At second a Ra–Be source — also placed in water — was simulated. The corresponding measured data were published by ALLEN [1960]. The space distribution of both the thermal and epithermal neutrons was studied. Epithermal neutrons were again measured by an indium foil. The relatively broad range, continuous initial energy-spectrum of the neutrons leaving the Ra–Be source had to be taken into account here (Fig. 1). Again, the program "recorded" the epithermal neutrons when they crossed the 1.44 eV energy level, while the threshold-energy of the thermal range was 0.1 eV. The results obtained from studying 9700 neutron-trajectories are presented in *Figs. 6* and *7*. Similarly to Fig. 5 the vertical axes represent the average number of neutrons on the 1 cm thick spherical shells at a distance r from the source but the scale is linear, as in the original publication. (The computed data were normalized in order to be matched to the curves: one unit was 350 neutrons for the epithermal neutrons and 37 500 neutrons for the thermal ones). Measured and computed data are represented by continuous lines and dots, respectively. Finally, similar computations were carried out for dry sandstone and for wet sandstone of 20% porosity. The corresponding data are to be found in [DENISHIK et al. 1962]. The source was also Ra–Be, the energy of the epithermal neutrons was 0.1 eV suited to the cadmium foil. 2400 neutrons were modelled in order to study their distribution in dry sandstone; *Fig. 8* shows the result. Measured and computed data — as averages for 15 cm thick spherical shells — are represented by a continuous line and dots, respectively. In the case of the 20% porosity wet sandstone the trajectories of approximately 1100 neutrons were simulated *(Fig. 9)*. Data concerning the thermal and epithermal distribution were also available so computations were performed for the thermal range, too. Computed data are averaged for 4 cm thick shells.

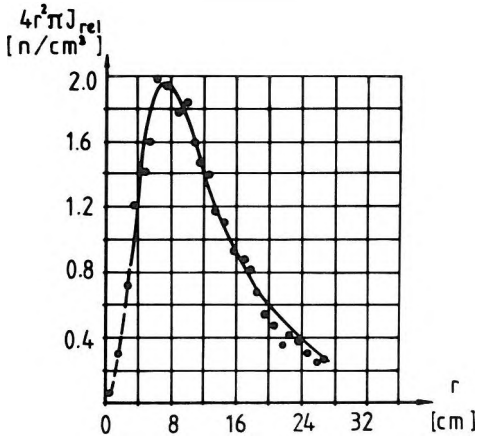

Fig. 6. Epithermal neutron distribution of Ra–Be neutron source measured in water by indium foil (continuous line) and computed by the simulation program (dots)

6. ábra. Ra–Be neutronforrás körüli epitermikus neutroneloszlás vízben, indium fóliával mérve (folytonos vonal), és a szimulációs programmal számítva (pontok)

Рис. 6. Распределение эпитермических нейтронов от источника Ra–Be в воде при измерении индиевой фольгой (сплошная линия) и при расчете симуляционной программой (пунктир).

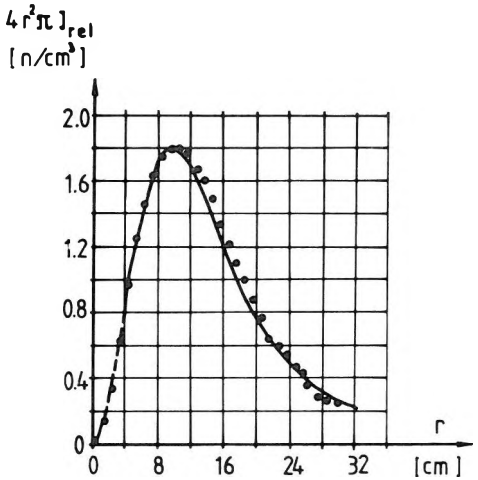

Fig. 7. Thermal neutron distribution of Ra–Be neutron source measured in water (continuous line) and computed by the simulation program (dots)

7. ábra. Ra–Be neutronforrás körüli termikus neutroneloszlás vízben mérve (folytonos vonal), és a szimulációs programmal számítva (pontok)

Рис. 7. Распределение термических нейтронов от источника Ra–Be, измеренное в воде (сплошная линия) и рассчитанное по симуляционной программе (пунктир).

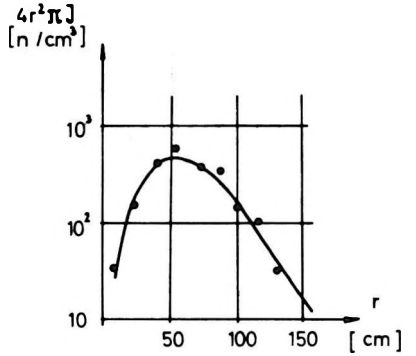

Fig. 8. Epithermal neutron distribution (energy 0.1 eV) around Ra–Be neutron source in dry sandstone (continuous line) and computed by the simulation program (dots)

8. ábra. Epitermikus, 0,1 eV energiájú neutronok eloszlása száraz homokkőben (folytonos vonal), és a szimulációs programmal számítva (pontok). Neutronforrás: Ra–Be

Рис. 8. Распределение эпитермических нейтронов с энергией 0,1 эв в сухом песчанике (сплошная линия) и рассчитанное по симуляционной программе (пунктир). Источник нейтронов — Ra–Be.

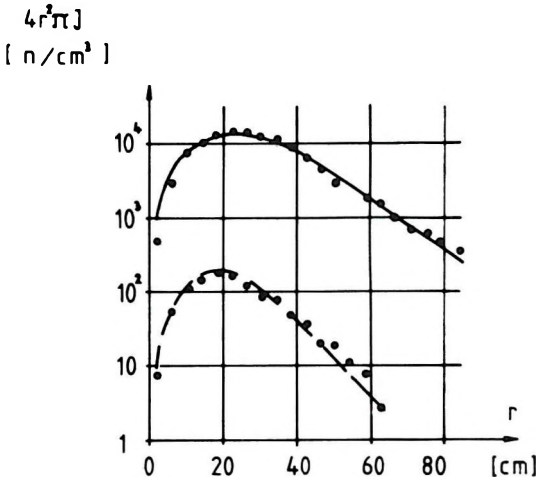

Fig. 9. Epithermal (energy ~0.1 eV, dotted line) and thermal (continuous line) neutron distributions around Ra–Be neutron source in 20% porosity wet sandstone, and computed by the simulation program (dots)

9. ábra. Epitermikus, 0,1 eV energiájú (szaggatott vonal), és termikus (folytonos vonal) neutronok eloszlása 20% porozitású vizes homokkőben, ill. a szimulációs programmal számítva (pontok). Neutronforrás: Ra–Be

Рис. 9. Распределение термических (сплошная линия) и эпитермических (штриховая линия) с энергией 0,1 эв, полученное в обводненных песчаниках с пористостью 20% и рассчитанное по симуляционной программе (пунктир). Источник нейтронов — Ra–Be.

5. Modelling the neutron field of ^{252}Cf in homogeneous isotropic bauxitic media

In bauxite well logging, instead of Ra–Be, ^{252}Cf neutron sources are used better suited to the requirements of neutron-activation measurements. The ^{252}Cf source produces neutrons by spontaneous fission, so the initial energy distribution of the emitted neutrons (N(E)) can be expressed analytically by the Maxwell distribution: $N(E) = \sqrt{E}\,e^{-E/T}$, where T is for ^{252}Cf: 1.43 MeV. [KARDON et al. 1971]. The ^{252}Cf spectrum of Fig. 1 was constructed with the help of this formula. The modelling program was run for pure water with the initial energy distribution of ^{252}Cf in order to compare the results with those of the Ra–Be source. The thermal neutron fields of the two sources in the form of the ratio of the number of neutrons in unit volume and the number of all neutrons modelled versus the distance from the source are presented in *Fig. 10*. This presentation relating to unit volumes meets better the conditions of well logging. As can be seen, both thermal neutron fields in pure water of both sources can be approximated linearly in logarithmic scale which means exponential distributions. It is also apparent that the softer spectrum of ^{252}Cf produces a steeper gradient (the average energy of Ra–Be is 3.6 MeV; that of ^{252}Cf is 2.05 MeV).

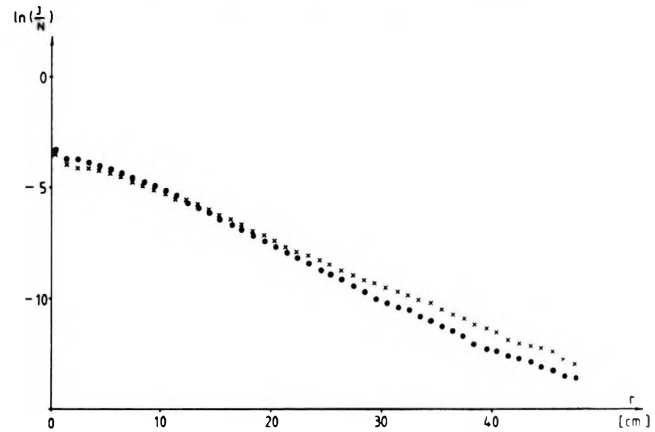

Fig. 10. Thermal neutron distributions around Ra–Be (calculated for 9,700 neutrons, x-es) and ^{252}Cf (calculated for 32,000 neutrons, dots) neutron sources in water, computed by the simulation program. On the vertical axis: logarithm of the ratio of neutrons in unit volume to all simulated neutrons

10. ábra. Termikus neutron eloszlások vízben, a szimulációs programmal számítva. x-ek: neutronforrás Ra–Be, 9700 neutronra számítva, pontok: neutronforrás ^{252}Cf, 32 000 neutronra számítva. A függőleges tengelyen az egységnyi térfogatra eső neutronok és az összes szimulált neutron hányadosának természetes logaritmusa

Рис. 10. Распределения термических нейтронов в воде, рассчитанные по симуляционной программе. Крестики — источник нейтронов Ra–Be, в расчете на 9700 нейтронов, пунктир — источник нейтронов ^{252}Cf в расчете на 32 000 нейтронов. По вертикальной оси отложены натуральные логарифмы отношений количеств нейтронов в единице объема к количеству всех симулированных нейтронов.

In other words it means that neutrons emitted from the ^{252}Cf source cover, on average, a somewhat shorter distance than the neutrons of the Ra–Be source.

In the following, calculations were performed on bauxites of differing composition, on clay, and on a mixture of bauxite and limestone detritus. The respective mineral and chemical compositions, densities and hydrogen-porosity data are to be found in *Tables II and III.* Mineral compositions were selected so that the main types of Hungarian bauxites should be represented [BÁRDOSSY 1977, BARNABÁS 1966]. The number of modelled neutrons was 10–11 thousand in each case. *Table IV.* and *Figures 11, 12* present the results for the epithermal between 0.1–1.0 eV and the thermal neutron flux respectively, normalized to unit source strength. Vertical axes are scaled for water, for the other media the coordinate system must be shifted.

Elements \ Rock code		0	1	2	3	4	5	6	7
Al	[g/cm³]	0	0.417	0.325	0.573	0.394	0.408	0.217	0.287
Si	[g/cm³]	0	0.011	0.169	0.028	0.197	0.085	0.225	0.014
Fe	[g/cm³]	0	0.195	0.329	0.391	0.329	0.438	0.574	0.195
Ti	[g/cm³]	0	0.012	0.024	0.024	0.024	0.024	0	0.012
Ca	[g/cm³]	0	0.005	0.011	0.011	0.011	0.005	0	0.543
S	[g/cm³]	0	0	0	0	0	0.351	0	0
C	[g/cm³]	0	0.002	0.003	0.003	0.003	0.002	0	0.163
O	[g/cm³]	0.888	1.222	1.242	1.296	1.268	1.09	1.237	1.296
H	[g/cm³]	0.112	0.093	0.074	0.07	0.066	0.07	0.068	0.036
Al_2O_3	[Dry weight %]	–	50.9	34.15	54.49	38.95	36.4	21.3	23.19
SiO_2	[Dry weight %]	–	1.56	20.12	3.03	22.06	8.54	25.1	1.29
Fe_2O_3	[Dry weight %]	–	18.05	26.15	28.13	24.59	29.55	42.74	11.97
TiO_2	[Dry weight %]	–	1.32	2.27	2.05	2.13	1.92	0	0.87
CaO	[Dry weight %]	–	0.49	0.84	0.76	0.79	0.36	0	32.51
Ignition loss	[Dry w. %]	–	27.69	16.46	11.54	11.48	23.22	10.85	30.17

Table III. Chemical composition of the modelled bauxitic rocks (elements and oxides referring to dry rock matrix, corresponding to laboratory chemical analysis)
For code numbers, see Table II.

III. táblázat. A modellezett bauxitos kőzetek kémiai összetétele, és száraz kőzetmátrixra vonatkoztatott oxidos összetétele (ez utóbbi megfelel a laboratóriumi vegyelemzésnek).
A kódszámokat lásd a II. táblázatban

Таблица III. Химический состав моделированных бокситов, исходный и пересчитанный на сухую породу в виде окислов; последний соответствует лабораторным определениям.
Кодовые номера см. в табл. II.

Analysis of the distributions of Figs. 11 and 12 enable one to conclude that in a homogeneous medium both the epithermal and thermal distributions may be well approached by exponential functions – or in logarithmic representation by straight lines. The linear relation seems to fit the best in the $r > 4$ cm range, which is the equivalent of the environment of the standard (76 mm) borehole diameter in bauxite prospecting in Hungary. The linear relation was also numerically examined in the 4–30 cm range. The Φ_{ep} epithermal flux is

$$\Phi_{ep} = F_1 \exp(-r/L_1)$$

that is

$$\ln \Phi_{ep} = \ln F_1 - (r/L_1)$$

For the Φ_t thermal flux

$$\Phi_t = F_2 \exp(-r/L_2)$$

that is

$$\ln \Phi_t = \ln F_2 - (r/L_2)$$

L_1 and L_2 can be related to the slowing down length (L_f) and the migration length (L_M), respectively [QUITTNER et al. 1971]. Constants given by regression calculation are in Table IV. Linear regression has proved to be adequately close in each case: the worst correlation factor was 0.99.

Rock code	Epithermal distribution		Thermal distribution	
	F_1 [10^{-4} n/s/cm^2]	L_1 [cm]	F_2 [10^{-2} n/s/cm^2]	L_2 [cm]
0	4.026	3.48	3.031	4.07
1	5.462	3.4	2.608	3.86
2	4.316	3.94	1.505	4.58
3	4.699	3.87	1.488	4.49
4	4.015	4.18	1.229	4.96
5	4.299	4.01	1.261	4.53
6	4.255	4.09	1.232	4.68
7	2.258	6.14	0.472	7.93

Table IV. Parameters of the exponential curves fitted to the epithermal and thermal neutron distributions of the ^{252}Cf neutron source between 4 and 30 cm (Figs. 11–12). For code numbers, see Table II.

IV. táblázat. A ^{252}Cf neutronforrás szimulált epitermikus és termikus neutroneloszlásaihoz (11–12. ábra) 4–30 cm között illesztett exponenciális görbék paraméterei. A kódszámokat lásd a II. táblázatban

Таблица IV. Параметры экспоненциальных кривых, полученных путем аппроксимации в интервале 4–30 см симулированных распределений эпитермических и термических нейтронов (рис. 11 и 12) источника ^{252}Cf. Кодовые номера см. в табл. II.

The L_f slowing down length increases with decreasing hydrogen content, if the rock composition is the same. This fact is taken advantage of by the dual-spaced neutron-porosity logging. *Figure 13* shows the relation between the L_1 data that were computed by regression from epithermal distributions and between the hydrogen content of a unit volume of the modelled media (H[g/cm^3]) and its hydrogen-porosity (P_H[%]). The relation has a hyperbolic tendency.

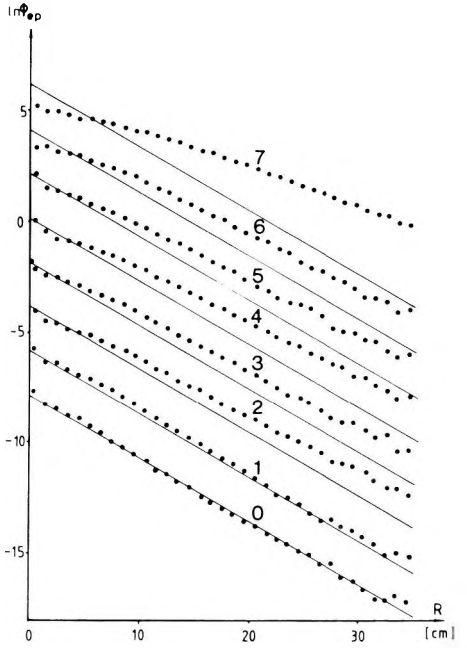

Fig. 11. Epithermal neutron flux around ^{252}Cf neutron source in water and in bauxitic rocks, computed by the simulation program. For code numbers, see Table II. The curves coded by 1–7 are in each case shifted by two units along vertical axis. The adjusted straight line of water (code number 0: see Table II) is also shifted for reference

11. ábra. Epitermikus neutronfluxus vízben és bauxitos kőzetekben, a szimulációs programmal számítva. Neutronforrás: ^{252}Cf, kódszámokat lásd a II. táblázatban. Az 1–7 kódszámú görbék a függőleges tengely mentén 2–2 egységgel el vannak tolva. Az eltolt görbék mellett referenciaként fel van tüntetve a 0 kódjelű víz kiegyenlítő egyenesének eltolt változata is

Рис. 11. Потоки эпитермических нейтронов в воде и в бокситах, рассчитанные по симуляционной программе. Источник нейтронов — ^{252}Cf, коды приводятся в табл. II. Кривые №№ 1–7 смещены вдоль вертикальной оси на 2 единицы каждая. Для сравнения рядом с ними нанесены смещенные прямые, соответствующие воде, обозначенной кодом 0.

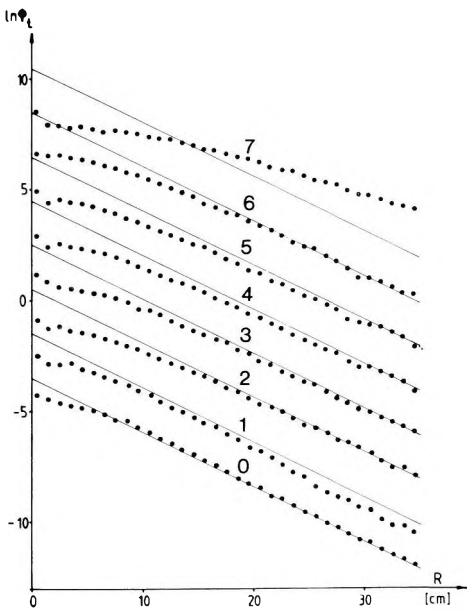

Fig. 12. Thermal neutron flux around ^{252}Cf neutron source in water and in bauxitic rocks, computed by the simulation program. Legend as in Fig. 11

12. ábra. Termikus neutronfluxus vízben és bauxitos kőzetekben, a szimulációs programmal számítva. Neutronforrás: ^{252}Cf, jelölések azonosak a 11. ábráéval

Рис. 12. Потоки термических нейтронов в воде и в бокситах, рассчитанные по симуляционной программе. Источник нейтронов — ^{252}Cf, обозначения см. на рис. 11.

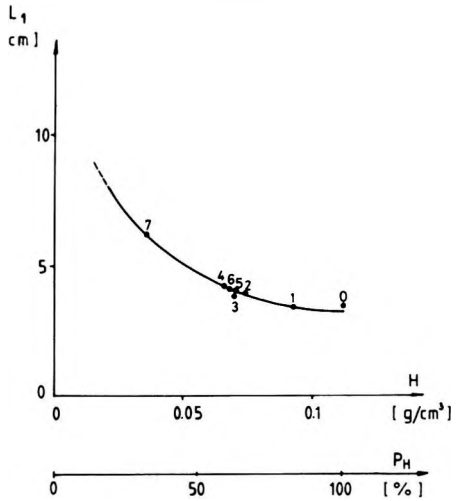

Fig. 13. Relation between the L_1 parameter of the exponential adjustment of the epithermal distributions (the reciprocals of gradients in Fig. 11) and hydrogen content (H) and hydrogen porosity (P_H) of the modelled medium. For code numbers, see Table II

13. ábra. Az epitermikus eloszlások exponenciális kiegyenlítő görbéinek L_1 paramétere (a 11. ábra görbemeredekségeinek reciproka) és a modellezett közeg hidrogéntartalma (H) ill. hidrogénporozitása (P_H) közötti kapcsolat. Kódszámokat lásd a II. táblázatban

Рис. 13. Взаимосвязь между параметром L_1 (величиной, обратной крутизнам кривых рис. 11) выравнивающих экспоненциальных кривых эпитермических распределений и содержанием водорода (H) в моделируемых породах и их водородной пористостью (P_H). Коды см. в табл. II.

6. Analysis of neutron fields simulated in homogeneous, isotropic bauxitic media

Let us examine the above discussed distributions more thoroughly. The following boundary condition is valid for epithermal flux due to the stationary neutron field (see Appendix):

$$\int_V q_{ep}\,\mathrm{d}V = \int_V \xi\Sigma_t\Phi_{ep}\,\mathrm{d}V = Q$$

that is

$$\int_V \xi\Sigma_t F_1 \exp\left(-r/L_1\right)\mathrm{d}V = Q$$

and so

$$8\pi\xi\Sigma_t F_1 L_1^3 = Q \tag{1}$$

where Q = intensity of the neutron field [n/s] (it was unity for the simulated fields)

q_{ep} = epithermal slowing down density [n/s/cm^3]

ξ = average logarithmic energy-decrease

Σ_t = macroscopic total (epithermal) cross-section [cm^{-1}]

$\xi\Sigma_t$ = slowing down power [cm^{-1}]

$\mathrm{d}V$ = volume element [cm^3]

A similar boundary condition is valid in the thermal range:

$$\int_V \Sigma_a \Phi_t \, dV = Q$$

that is

$$\int_V \Sigma_a F_2 \exp(-r/L_2) \, dV = Q$$

and so

$$8\pi \Sigma_a F_2 L_2^3 = Q, \tag{2}$$

where Σ_a is the macroscopic absorption (thermal) cross-section [cm^{-1}].

The dimension of flux and thus of F is [$n/s/cm^{-2}$]. Let us now consider the L_1 and L_2 quantities. The following relation exists between the slowing down length, L_f, and the migration length, L_M, [QUITTNER et al. 1971]:

$$L_M^2 = L_f^2 + L_d^2,$$

where L_d is the thermal diffusion length [cm].

The following relation is also known [SZATMÁRY 1971]:

$$L_d^2 = 1/(3\Sigma_s \Sigma_a),$$

where Σ_s is the macroscopic scattering (thermal) cross-section [cm^{-1}].

Bearing in mind the above-mentioned relations:

$$L_M^2 - L_f^2 = 1/(3\Sigma_s \Sigma_a).$$

Since the slowing down and migration lengths, L_f and L_M, may correspond to L_1 and L_2, we obtain:

$$L_2^2 - L_1^2 = 1/(3\Sigma_s \Sigma_a). \tag{3}$$

Note that on the basis of the numbered equations—or in other words analysing the epithermal and thermal neutron distributions—the macroscopic cross-sections $\xi\Sigma_t$, Σ_s and Σ_a can be determined if Q, L_1, F_1, L_2 and F_2 are known. Thus, these might be considered as quasi-measurement data, obtained by measuring the neutron distribution. Data computed this way will be marked with an asterisk.

The above macroscopic cross-sections may also be directly calculated from the microscopic cross-sections [NAGY 1971, NIKOLAYEV and BAZAZYANTS 1972, and ALLEN 1960] if the chemical composition of the medium is known (Table III). Therefore the macroscopic cross-sections are linear combinations of the concentrations of elements. *Table V* contains the macroscopic cross-sections determined in two different ways — from quasi-measurement and from the chemical composition. The average of the total cross-section of hydrogen in the fast range was needed to calculate the slowing down power (see Appendix). This value was calculated by means of simulation for water. Consequently, the slowing down power of water computed from the chemical composition is based on quasi-measurement only, therefore this value was also marked with an

Rock code	Epithermal distribution		Thermal distribution			
	macroscopic cross-section		scattering		absorption	
	$\xi\Sigma_t$ [cm^{-1}]	$\xi\Sigma_t^*$ [cm^{-1}]	Σ_s [cm^{-1}]	Σ_s^* [cm^{-1}]	Σ_a [cm^{-1}]	Σ_a^* [cm^{-1}]
0	2.355*	2.355	2.012	3.81	0.0221	0.0194
1	1.971	1.855	1.79	3.749	0.0269	0.0265
2	1.577	1.510	1.497	2.209	0.0278	0.0275
3	1.493	1.461	1.447	2.168	0.0295	0.0295
4	1.398	1.356	1.361	1.77	0.0265	0.0266
5	1.475	1.433	1.411	2.235	0.0334	0.034
6	1.446	1.366	1.417	2.037	0.0309	0.0314
7	0.772	0.76	0.898	0.786	0.0184	0.0169

Table V. Neutron-physical parameters, calculated from the chemical composition of modelled bauxitic rocks (Table III) and from neutron distributions (marked with asterisk). For code numbers, see Table II.

V. táblázat. Neutronfizikai paraméterek a modellezett bauxitos kőzetek kémiai összetételéből (III. táblázat), illetve a szimulált neutroneloszlásokból (csillaggal jelölve) számítva. A kódszámokat lásd a II. táblázatban

Таблица V. Нейтронно-физические параметры, рассчитанные по химическому составу бокситов (табл. III) и по симулированным распределениям нейтронов, обозначенным звездочкой. Кодовые номера см. в табл. II.

asterisk in the Table. Naturally the slowing down powers computed from the chemical compositions of the other media are independent of the quasi-measured data concerning the given media.

The data of Table V are graphically illustrated by *Figs. 14, 15* and *16*. The code number of the given medium (see Table II) is indicated at each point. It can be seen that data calculated from the quasi-measurements and from the

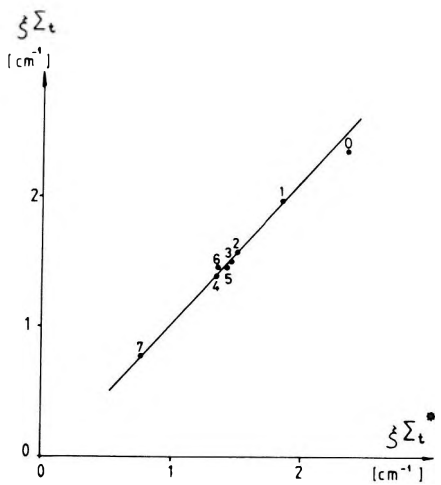

Fig. 14. Relation between *slowing down powers* $\xi\Sigma_t^*$ calculated from Formula (1) and $\xi\Sigma_t$ calculated from the chemical composition. For code numbers, see Table II

14. ábra. Az elemi összetételből számított $\xi\Sigma_t$, és a (1) összefüggés alapján számított $\xi\Sigma_t^*$ *fékezési erély* kapcsolata. A kódszámokat lásd a II. táblázatban

Рис. 14. Взаимосвязь между $\xi\Sigma_t$, рассчитанным по элементному составу, и *тормозящим моментом* $\xi\Sigma_t^*$, рассчитанным по выражению (1). Коды см. в табл. II.

chemical composition agree well; data of the macroscopic scattering even show a close correlation. Only the data of water denoted by code-number 0 and, in case of the scattering cross-section, the bauxite mixed with detrital limestone denoted by 7 fall slightly off the averaging straight line.

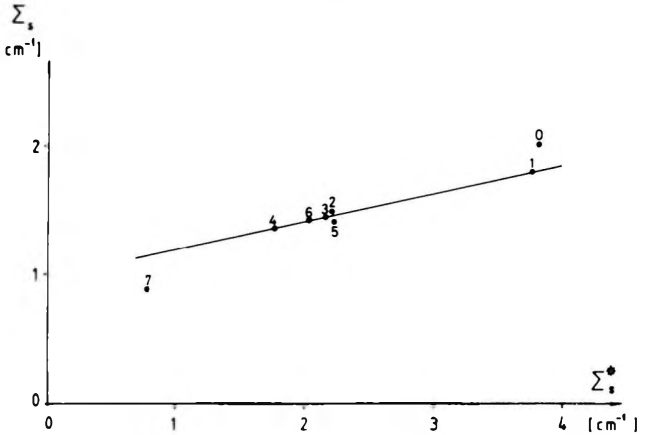

Fig. 15. Relation between *scattering cross section* Σ_s^* computed from Formula (2) and Σ_s calculated from the chemical composition. For code numbers, see Table II

15. ábra. Az elemi összetételből számított Σ_s, és a (2) összefüggés alapján számított Σ_s^* *szórási hatáskeresztmetszetek* kapcsolata. A kódszámokat lásd a II. táblázatban

Рис. 15. Взаимосвязь между Σ_s, рассчитанным по элементному составу, и *диффузионным эффективным сечением* Σ_s^*, рассчитанным по выражению (2). Коды см. в табл. II.

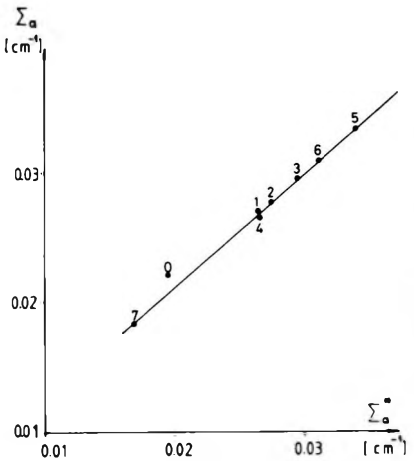

Fig. 16. Relation between *absorption cross-section* Σ_a^* calculated from Formula (3) and Σ_a calculated from the chemical composition. For code numbers, see Table II

16. ábra. A (3) összefüggés alapján számított Σ_a^* *abszorpciós hatáskeresztmetszetek* és az elemi összetételből számított Σ_a kapcsolata. A kódszámokat lásd a II. táblázatban

Рис. 16. Взаимосвязь между *абсорбционным эффективным сечением* Σ_a^*, рассчитанным по выражению (3), и Σ_a, рассчитанным по элементному составу. Коды см. в табл. II.

7. Simulation of neutron fields in bauxitic media taking into account the probe and the borehole

The main advantage of the Monte Carlo method in simulating neutron fields is that any arbitrary geometry may be assumed in the given medium — as was mentioned in the introduction. Using this possibility, let us see how the presence of the probe and the borehole influences the homogeneous, isotropic fields. An R–Z coordinate system was set up for the new calculations in which the probe and the borehole are positioned concentrically around the Z-axis; the diameter of the probe and the borehole are 40 and 80 mm, respectively. The studied volume of space extends 100 cm in the Z direction and 40 cm in the R direction. It was sufficient to record the neutron-physical events in $40 \times 100 = 4000$ elementary cells due to cylindrical symmetry. The ^{252}Cf radioactive source was at the origin of the coordinate system. The body of the probe was assumed to be iron but only half of its density was used in the calculations thus modelling the approximately 50% material/volume ratio of the probe structure. The probe extends 15 cm below the origin and extends along the whole studied volume of space upwards. In the first version of the calculations the hole is filled with water, in the second one it is dry. The medium is gibbsitic bauxite (code number 1 in Table II). This rock was selected for studying the influence of the probe and borehole because its neutron-physical parameters differ the most from the same of the probe and the dry hole and so the distorting effect is expected to be the strongest in this case. Naturally, the hole filled with water will not have a very strong distorting effect.

The arrangement and the results for water-filled boreholes are shown by *Figs. 17* and *18*. Cells having neutrons are inside the contour. Those cells in which the logarithm of the neutron density corresponding to unit neutron yield is greater than -12.5, are shaded horizontally, while vertical shading means those cells in which this logarithm is greater than -10. The distribution of epithermal neutrons of 0.1 eV energy is presented in Fig. 17, and the same for absorbed thermal neutrons in Fig. 18. The number of neutrons in the study was approximately 38 thousand. This number was not enough for an accurate, quantitative analysis of the neutron-distribution—as is suggested by the figures—though the maximum capacity of the Commodore 64 was used. Nevertheless, the figures are still suitable for qualitative analysis. The distortion caused by the sonde-body in the Z direction is apparent — especially in the case of the epithermal neutrons. It is also interesting that the epithermal neutrons hardly penetrate into the sonde-body. *Figure 19* showing the distribution of the thermal neutron flux along the Z axis, allows a comparison with the homogeneous isotropic field. The coordinate-system is identical with that of Fig. 12 and so the corresponding homogeneous isotropic data could be displayed along the data measured in an inhomogeneous field. The position of the ^{252}Cf source and the probe is also shown along the Z axis.

Figures 20–22 are similar to the previous ones with the difference that here the borehole was dry. The distorting effect in the Z direction increased.

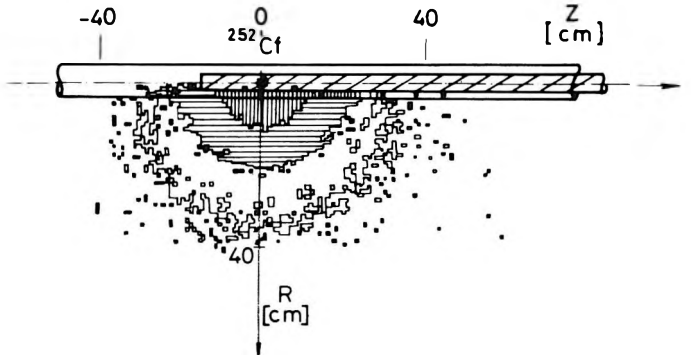

Fig. 17. Distribution of epithermal neutrons (energy ~0.1 eV) around a ^{252}Cf neutron source in *water-filled* borehole drilled in gibbsitic bauxite

17. ábra. Epitermikus, 0.1 eV energiájú neutronok eloszlása gibbszites bauxitot harántoló *vizes* fúrólyukban. Neutronforrás: ^{252}Cf

Рис. 17. Распределение эпитермических нейтронов с энергией 0,1 эв в *обводненной* скважине, вскрывшей гиббситовые бокситы. Источник нейтронов — ^{252}Cf.

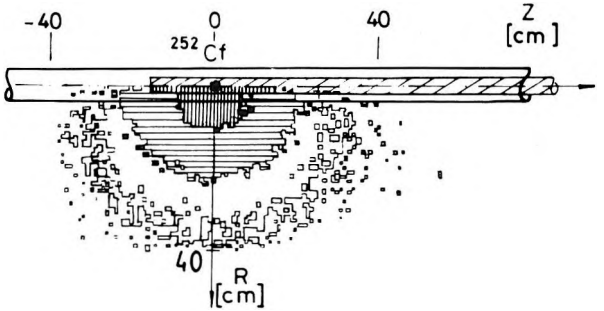

Fig. 18. Distribution of absorbed thermal neutrons around the ^{252}Cf neutron source in *water-filled* borehole drilled in gibbsitic bauxite

18. ábra. Abszorbeálódott termikus neutronok eloszlása gibbszites bauxitot harántoló *vizes* fúrólyukban. Neutronforrás: ^{252}Cf

Рис. 18. Распределение абсорбированных термических нейтронов в *обводненной* скважине, вскрывшей гиббситовые бокситы. Источник нейтронов — ^{252}Cf.

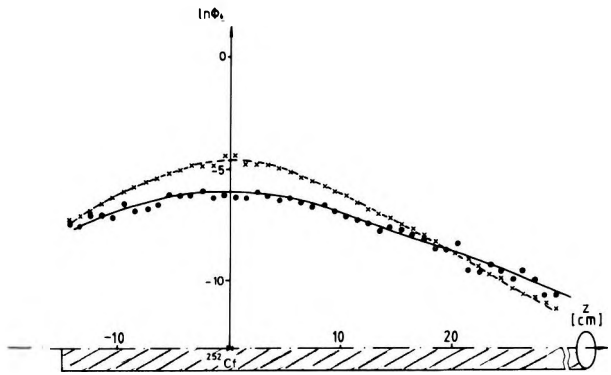

Fig. 19. Thermal neutron flux of a ^{252}Cf neutron source along the axis of the probe, in *water-filled* borehole drilled in gibbsitic bauxite (x-es mark the distribution computed for to the homogeneous isotropic medium)

19. ábra. Termikus neutronfluxus gibbszites bauxitot harántoló *vizes* fúrólyukban, a szonda tengelye mentén. Neutronforrás: ^{252}Cf (x-ek a homogén izotróp közegre számított eloszlást jelölik)

Рис. 19. Потоки термических нейтронов в *обводненной* скважине, вскрывшей гиббситовые бокситы, вдоль оси зонда. Источник нейтронов — ^{252}Cf (крестиками обозначено распределение, рассчитанное для однородной изотропной среды).

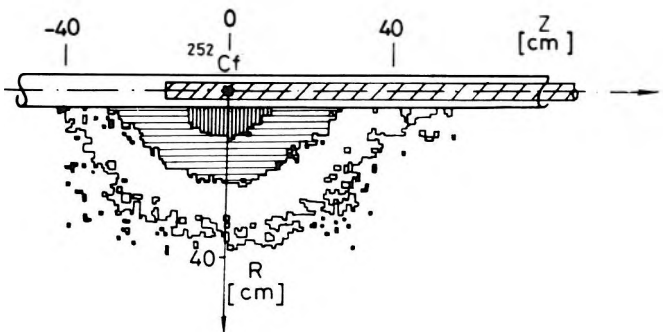

Fig. 20. Distribution of epithermal neutrons of 0.1 eV energy around the ^{252}Cf neutron source in *dry* borehole drilled in gibbsitic bauxite

20. ábra. Epitermikus, 0,1 eV energiájú neutronok eloszlása gibbszites bauxitot harántoló *száraz* fúrólyukban. Neutronforrás: ^{252}Cf

Рис. 20. Распределение эпитермических нейтронов с энергией 0,1 эв в *сухой* скважине, вскрывшей гиббситовые бокситы. Источник нейтронов — ^{252}Cf.

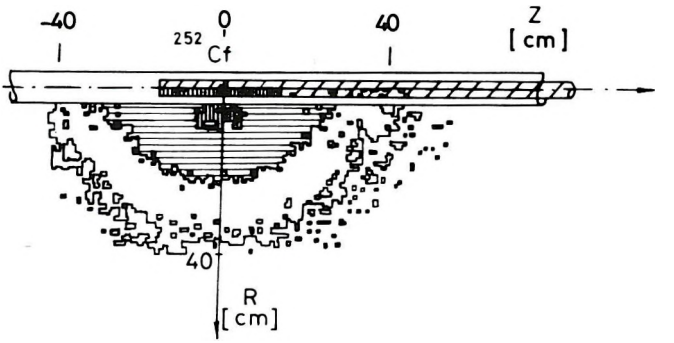

Fig. 21. Distribution of absorbed thermal neutrons around the ^{252}Cf neutron source in *dry* borehole drilled in gibbsitic bauxite

21. ábra. Abszorbeálódott termikus neutronok eloszlása gibbszites bauxitot harántoló *száraz* fúrólyukban. Neutronforrás: ^{252}Cf

Рис. 21. Распределение абсорбированных термических нейтронов в *сухой* скважине, вскрывшей гиббситовые бокситы. Источник нейтронов — ^{252}Cf.

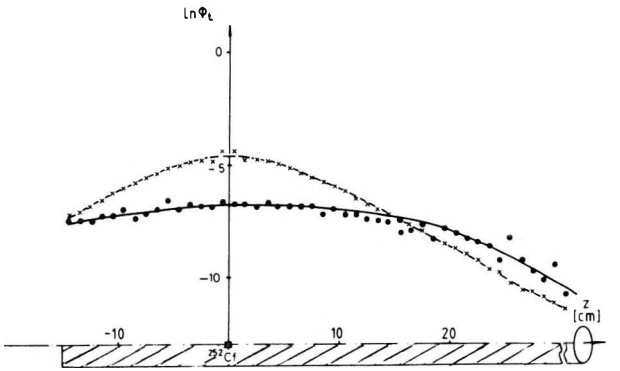

Fig. 22. Thermal neutron flux of a ^{252}Cf neutron source along the axis of the probe in *dry* borehole drilled in gibbsitic bauxite (x-es mark the distribution computed for to the homogeneous isotropic medium)

22. ábra. Termikus neutronfluxus gibbszites bauxitot harántoló *száraz* fúrólyukban, a szonda tengelye mentén. Neutronforrás: ^{252}Cf (x-ek a homogén izotróp közegre számított eloszlást jelölik)

Рис. 22. Потоки термических нейтронов в *сухой* скважине, вскрывшей гиббситовые бокситы, вдоль оси зонда. Источник нейтронов — ^{252}Cf (крестиками обозначено распределение, рассчитанное для однородной изотропной среды).

8. Conclusions

It has been proved that the Monte Carlo modelling program presented here is suitable for studying neutron fields developing in media of many chemical components or of complicated geometry. The program is also able to study the effect of layering. Nevertheless in order to solve such tasks of complicated geometry quantitatively, a faster computer with bigger memory—than the Commodore 64—is needed. Even so, it can be concluded from our computations that the epithermal and thermal neutron fields can be approximated by exponential functions in media of high hydrogen content. These media may be —besides bauxitic rocks—laterites, coals, clays or kaoline.

This exponential approach may be used to correct neutron-activation measurements—as was discussed earlier [Balogh and Horváth 1983]—and on the other hand it may help the interpretation of spectral neutron-gamma measurements [Chrusciel et al. 1985], i.e. it could render a possibility to take into account the influence of neutron distribution on the measurements. The exponential distribution also renders the in situ measurement of the $\xi\Sigma_t$, Σ_s and Σ_a neutron-physical parameters possible in rocks of high hydrogen content by profiling of the epithermal and thermal neutron fields by two times two (two epithermal and two thermal) detectors. It has been proven [Flaum 1983] that it is possible to construct a suitable tool; he reports on the realization of such a tool for hydrogen porosity determination in dry boreholes. To decrease the distorting effects and to be able to detect the epithermal neutrons the body of such a tool should be made of some plastic of high hydrogen content and it should be pressed against the wall of the hole. The parameters measured in this way will be linearly related to the chemical composition of rocks, which is the most important feature to be learnt when prospecting for solid minerals.

APPENDIX

It is known that the slowing down density in media which do not absorb neutrons is as follows [Szatmáry 1971]:

$$q(r, E) = \int_{E'=E}^{E/\alpha} \Sigma_t(E') \frac{E - E'\alpha}{E'(1-\alpha)} \Phi(r, E')\, \mathrm{d}E'$$

where $\alpha = (A-1)/(A+1)$

A = atomic weight

since Σ_t is the sum of the cross-sections of the i components, the integral can be divided

$$q(r, E) = \int_{E'=E}^{E_0} \Sigma_t^{\text{hydrogen}}(E') E \Phi(r, E') \frac{\mathrm{d}E'}{E'} + \sum_i \int_{E'=E}^{E/\alpha_i} \Sigma_t^i(E') \frac{E - E'\alpha_i}{E'(1-\alpha_i)} \Phi(r, E')\, \mathrm{d}E'$$

Here it was taken into account that $\alpha = 0$ for hydrogen. For the other rock-forming elements $\alpha_i \approx 1$, thus the integral can be simplified [SZATMÁRY 1971]:

$$q(r, E) = \int_{E'=E}^{E_0} \Sigma_t^{\text{hydrogen}}(E') E\Phi(r, E') \frac{dE'}{E'} + \sum_i \Sigma_t^i(E) \xi_i E\Phi(r, E)$$

It is usually accepted to decompose the flux to two factors, one depending on the position and the other on the energy [SZATMÁRY 1971]:

$$\Phi(r, E) = R(r)F(E).$$

If it is assumed that the function of energy $F(E)$ is nearly constant in bauxitic rocks, this expression can be written in the following form

$$q(r, E) = \bar{\Sigma}_t^{\text{hydrogen}} E\Phi(r, E) + \sum_i \Sigma_t^i(E) \xi_i E\Phi(r, E)$$

where

$$\bar{\Sigma}_t^{\text{hydrogen}} = \frac{R(r) \int_{E'=E}^{E_0} \Sigma_t^{\text{hydrogen}}(E') F(E') \, dE'/E'}{R(r)F(E)}$$

This quantity will be constant because $F(E)$ was assumed to be constant. If the overstroke is omitted and instead of $E\Phi(r, E)$ $\Phi_{ep}(u, r)$ is written, and if it is considered that $\xi(\text{hydrogen}) = 1$ then:

$$q_{ep} = \sum_i \Sigma_t^i \xi_i \Phi_{ep}(u, r) = \xi \Sigma_t \Phi_{ep}$$

where $u = \ln (E_0/E)$.

Note: if $F(E)$ changes then this equation will only approximately be valid because $\Sigma_t^{\text{hydrogen}}$ was assumed constant. The accuracy of the approximation depends on $F(E)$. However, our modelling results support the assumption of $F(E) \approx$ const. in the studied rocks.

REFERENCES

ALLEN W. D. 1960: Neutron detection. Newnes LTD., London, 260 p.

BALOGH I., HORVÁTH J. 1983: Quantitative determination of Al_2O_3 content in bauxite-prospecting boreholes by means of neutron-activation logging. Geophysical Transactions, **29**, 2, pp. 173–185

BARNABÁS K. 1966: Bauxite. In: The geology of our mineral deposits (in Hungarian). Ed.: B. Jantsky, Műszaki Kiadó, Budapest, pp. 143–178

BÁRDOSSY GY. 1977: Karst bauxites (in Hungarian). Akadémiai Kiadó, Budapest 413 p.

BETECHTIN A. G. 1964: Lehrbuch der Speziellen Mineralogie. VEB Deutscher Verlag für Grundstoffindustrie, Leipzig, 679 p.

Chrusciel E., Palka K., Kaczmarski S., Wojda F. 1985: Determination of coal properties in boreholes by neutron capture and backscattered gamma radiation spectrometry (in Russian). Proceedings of the 30th International Geophysical Symposium, Moscow, Vol B, 3, pp. 51–63

Denishik S. A., Rezvanov R. A., Lukhminszkij B. E. 1962: The method of statistic tests applied to the computation of the distribution of neutrons in problems of the neutron logging. In: Portable neutron generators in nuclear geophysics (in Russian). Editor: Savochin S. I., Publ. H. "Gosatomizdat", Moscow, pp. 172–202

Fehér S. 1984: Methods for computing neutron radiation fields. In: Electron shell and nuclear physics in the exploration of fluids and minerals in deep boreholes (in Hungarian). Ed.: Ferenczy L., Association of Hungarian Geophysicists, Csopak, pp. 109–160

Flaum C. 1983: Dual detector neutron logging in air filled boreholes. SPWLA Twenty-fourth annual logging symposium transactions, Vol. II., BB, 21 p.

Kardon B., Koltay E., Makra Zs. 1971: Neutronsources (in Hungarian). In: Neutronphysics. Ed.: D. Kiss, P. Quittner. Akadémiai Kiadó, Budapest pp. 49–130

Khisamutdinov A. I., Starikov V. N., Morozov A. A. 1985: The Monte Carlo algorithm in nuclear geophysics (in Russian). Publ. H. "Nauka", Novosibirsk, 157 p.

Nagy S. 1971: Neutron source- and absorption-application in chemical analysis (in Hungarian). In: Neutronphysics. Ed.: D. Kiss, P. Quittner. Akadémiai Kiadó, Budapest, pp. 941–952

Nikolayev M. N., Bazazyants N. O. 1972: The anisotropy of the elastic scattering of neutrons (in Russian). Publ. H. "Atomizdat", Moscow, 236 p.

Pshenichnyy G. A. 1982: Interaction between radiation and substance and modelling problems of nuclear geophysics (in Russian). Publ. H. "Energizdat", Moscow, 221 p.

Quittner P., Bata L., Deme S., Makra Zs., Nagy T., Somogyi Gy. 1971: Neutron-detection (in Hungarian). In: Neutronphysics. Ed.: D. Kiss, P. Quittner. Akadémiai Kiadó, Budapest, pp. 131–256

Radiation sources for laboratory and industrial use. 1974. (Catalogue 1974/75). Radiochemical Centre, Amersham, 99 p.

Szabó E., Simonits A. 1973: Activation analysis (in Hungarian). Műszaki Kiadó, Budapest, 362 p.

Szatmáry Z. 1971: Neutrongas-physics (in Hungarian). In: Neutronphysics. Ed.: D. Kiss, P. Quittner. Akadémiai Kiadó, Budapest, pp. 809–870

Szobol I. M. 1981: The basics of the Monte Carlo methods (in Hungarian). Műszaki Kiadó, Budapest, 318 p.

Yermakov S. M. 1975: The Monte Carlo method and adjacent problems (in Russian). Publ. H. "Nauka", Moscow, 472 p.

A ^{252}Cf NEUTRONFORRÁS TERÉNEK SZÁMÍTÓGÉPES SZIMULÁCIÓJA A BAUXITKAROTÁZSBAN

BALOGH Iván

A dolgozat a neutronterek eloszlását vizsgálja a neutrontranszport számítógépes szimulációjára alapozva, nagy hidrogéntartalmú – elsősorban bauxitos – kőzetekben. Röviden ismerteti a kidolgozott szimulációs (Monte Carlo) programot, majd le is teszteli publikációkból ismert mérési adatok segítségével. A dolgozat a továbbiakban tipikus bauxitos kőzetekre végzett számítások eredményeit ismerteti, amelyek szerint az adott kőzetekben az epitermikus és termikus neutronok exponenciális eloszlásúak. Megmutatja, hogy az epitermikus és termikus neutroneloszlások ismeretében kiszámíthatók a $\xi\Sigma_t$, Σ_s, Σ_a neutronfizikai paraméterek, melyek közvetlen lineáris kapcsolatban állnak az adott közeg elemi összetételével. Végül kvalitativ jellegű eredményeket mutat be a szondatest és a vizes, ill. száraz fúrólyuk neutronteret torzító hatásáról.

СИМУЛЯЦИЯ ПОЛЯ НЕЙТРОННОГО ИСТОЧНИКА ^{252}Cf В БОКСИТОВОМ КАРОТАЖЕ С ПОМОЩЬЮ ЭВМ

Иван БАЛОГ

В статье исследуется распределение нейтронных полей на основе симуляции на ЭВМ нейтронного транспорта в породах с большим содержанием водорода, в первую очередь в бокситовых породах. Кратко излагается выработанная программа симуляции Монте Карло, которая тестируется с помощью известных по литературе данных измерений, далее излагаются результаты расчётов по типичным бокситовым породам по которым резонансные и тепловые нейтроны имеют степенное распределение. Показывается, что зная распределение резонансных и тепловых нейтронов, можно рассчитать нейтронно-физические параметры $\xi\Sigma_i$, Σ_s, Σ_a, которые имеют непосредственную линейную связь с элементным составом данной среды. Наконец в статье представляются качественные результаты по искажающему влиянию на нейтронное поле обводенных и сухих скважин и корпуса зонда.